Influence of the aortic valve leaflets on the fluid-dynamics in aorta in presence of a normally functioning bicuspid valve

D. Bonomi[1] · C. Vergara[1] · E. Faggiano[1,2] · M. Stevanella[3] · C. Conti[4] · A. Redaelli[3] · G. Puppini[5] · G. Faggian[6] · L. Formaggia[1] · G. B. Luciani[6]

Received: 7 November 2014 / Accepted: 22 April 2015 / Published online: 6 May 2015

✉ C. Vergara
christian.vergara@polimi.it

D. Bonomi
diana.bonomi@polimi.it

[1] MOX, Dipartimento di Matematica, Politecnico di Milano, Piazza Leonardo da Vinci 32, 20133 Milan, Italy

[2] LaBS, Dipartimento di Chimica, Materiali e Ingegneria Chimica, Politecnico di Milano, Milan, Italy

[3] Dipartimento di Elettronica, Informazione e Bioingegneria, Politecnico di Milano, Milan, Italy

[4] EnginSoft SpA, Parco Scientifico Tecnologico Kilometro Rosso, Bergamo, Italy

[5] Department of Radiology, Azienda Ospedaliera Universitaria Integrata di Verona, Polo Confortini, Verona, Italy

[6] Division of Cardiac Surgery, Department of Surgery, University of Verona, Verona, Italy

1 Introduction

Bicuspid aortic valves (BAV) provide in general a normal circulatory physiology in absence of other complications, such as aortic valve pathology, aortic aneurysm, or dissection. However, they are associated with an increased prevalence of ascending aortic dilatation and, possibly, aneurysm in com-parison with a normally functioning tricuspid aortic valve (TAV) (Hahn et al. 1992; Fedak et al. 2002; Nkomo et al. 2003; Bauer et al. 2006). The reasons for this are matter of controversy: On the one hand, it is believed that a genetic ori-gin could lead to a weakening of the aortic wall (Guntheroth 2008); on the other hand, a crucial role seems to be played by the systolic blood fluid-dynamics observed in the ascending aorta in BAV cases (Barker and Markl 2011; Girdauskas et al. 2011), where the described fluid-dynamics is characterized by nonstandard features in comparison with one generated by a normally functioning TAV. In particular, the fluid-dynamics at systole in the ascending aorta in a normally functioning BAV feature:

1. An eccentric jet exiting from the left ventricle;
2. High concentrated wall shear stresses (WSS);
3. Elevated retrograde flows;
4. A possible helical flow, which becomes particularly intense in dilated cases.

These phenomena have been observed with medical imaging techniques, such as echocardiography (Schapira et al. 1979; Donal et al. 2005b) or phase-contrast magnetic resonance (PC-MRI) (Hope et al. 2014, 2010; Den Reijer et al. 2010; Barker et al. 2010; Hope et al. 2011; Sigovan et al. 2011; Barker et al. 2012), with in vitro experiments (Saikrishnan et al. 2012; Atkins et al. 2014; Keshavarz-Motamed et al. 2014), and with computational models (Viscardi et al. 2010; Vergara et al. 2012; Della Corte et al. 2012; Chan-dra et al. 2012; Pasta et al. 2012; Faggiano et al. 2013). In particular, in (Faggiano et al. 2013), we observed that the four characteristics of the BAV fluid-dynamics men-tioned above are not independent and are strictly related to one another. In (Viscardi et al. 2010; Vergara et al. 2012; Faggiano et al. 2013), rigid wall simulations where the valve orifice was projected on the valve plane (interface between left ventricle and aorta) and without modeling the leaflets were presented. These simulations highlighted that the shape and the area of BAV seem to be enough to repro-duce the abnormal fluid-dynamics in the ascending aorta with a satisfying accuracy (see Faggiano et al. (2013) for a quantitative comparison with 2D CINE PC-MRI data). However, in (Della Corte et al. 2012; Chandra et al. 2012; Marom et al. 2013b; Pasta et al. 2012) the importance of including the valve leaflets in the computational model has been highlighted to accurately describe the jet deflection and WSS.

In this paper, we present a work aimed at investigat-ing and quantifying the effect of the inclusion of the valve leaflets on the fluid-dynamic abnormalities experienced in BAV patients through unsteady fluid-dynamic numerical simulations with rigid walls and physiological inlet veloc-ity conditions. In particular, we aimed at comparing BAV and TAV configurations in presence of the leaflets, and BAV configurations with and without leaflets. To this end, some indices measuring jet asymmetry, flow reversal, heli-cal flow, and maximum wall shear stress were computed at the systole. We performed this comparison in two real geometries representing two different classes of ascending aortas, namely the non-dilated and the dilated (however non-aneurysmatic) cases. This choice has been supported by the observation that the abnormalities experienced in the fluid-dynamics of BAV patients are characterized by different intensities, in particular, they are higher in the dilated case. Thus, the inclusion of the leaflets could have in principle a different impact on the dilated and non-dilated cases.

2 Methods

2.1 Data acquisition and generation of the volumes

In this work, we considered two patient-specific non-stenotic BAV cases, one characterized by a normal ascending aorta (in what follows referred to as Patient 1), and the other one by a dilated ascending aorta with a diameter greater than 4 cm (referred to as Patient 2). Both patients featured an anteroposterior (AP) orientation of the commissures. None of the patients was affected by additional structural diseases, including aortic coarctation or tetralogy of Fallot.

For both patients, a 3D contrast-enhanced MRI (CE-MRI) was acquired with a voxel resolution of $1.72 \times 1.72 \times 1.5$ mm. The following parameters were used: TE (echo time) = 1.02 ms; flip angle = 20° ; slice thickness = 1.5 mm; acquisition matrix = 256 × 106. The two geometries are shown in Fig. 1. Two cross sections are considered at two different aortic levels, namely the *sinotubular junction* and the *mid-ascending aorta*. We will refer to these sections as A1 and A2, respectively (see Fig. 1).

Moreover, a breath-hold true fast imaging with steady-state precession (TrueFisp) cine-sequence with retrogated ECG triggering was acquired on the valve plane, defined as the interface between the left ventricle and the aorta, with the following parameters: TE (echo time) = 1.6 ms; flip angle = 65° ; slice thickness = 8 mm; temporal resolution = 20 phases in one cardiac cycle; acquisition matrix = 256 × 146.

All the MRI acquisitions were performed on a 1.5 Tesla system (Magnetom Symphony, Siemens Medical Systems, Erlangen, Germany).

A surface model of the aortic root, ascending aorta, and aortic arch of the two patients has been then generated from the 3D CE-MRI images, using a level set segmentation technique implemented in the open-source code Vascular Modeling Toolkit (*vmtk*, http://www.vmtk.org). The surfaces have been then cut at the aortic valve planes and at the outlets, obtaining the starting volumes (see Fig. 1).

2.2 Leaflets geometry

To include the leaflets in our geometries, we preliminarily performed two structural simulations in a realistic but not specific geometry, one for a BAV and one for a TAV configuration. To this aim, finite element models of BAV and TAV configurations were based on average dimensions derived from 2D MRI acquisitions performed on 10 TAV and 8 AP-BAV subjects, respectively (Conti et al. 2010). The mechanical response of aortic leaflets, modeled as a shell,

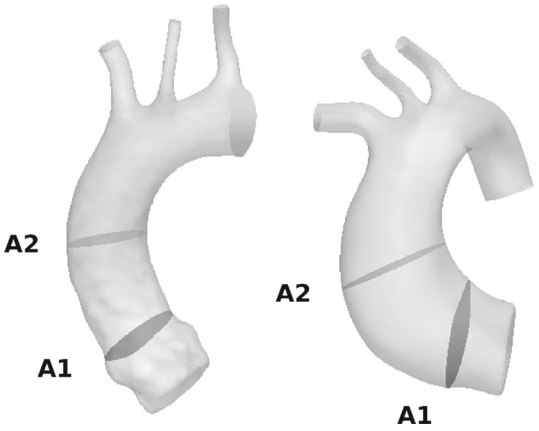

Fig. 1 Computational domains. *Left* Patient 1 with STJ (A1) and mid-ascending aorta (A2) sections; *Right* Patient 2 with sections A1 and A2

was described via a transversely isotropic incompressible hyperelastic model, implemented into the ABAQUS/Explicit code (ABAQUS/Explicit, SIMULIA Inc.) with a VUMAT subroutine, based on the following strain energy function (May-Newman and Yin 1998):

$$W = c_0 \exp\left(c_1(I_1 - 3)^2 + c_2(I_4 - 1)^2 - 1\right), \qquad (1)$$

where I_1 and I_4 are the first and fourth invariants of the Cauchy–Green strain tensor. Constants c_0, c_1, c_2 were set by fitting with the model reported by (Billiar and Sacks 2000). Constitutive materials of the aorta were assumed linear, elas-tic, and isotropic. The density was set equal to 1.1 g/mm^3 for all tissues. A two-step simulation was performed on the model. First, the aortic root was pressurized by a linearly increasing load from the zero-pressure state to the telediastolic aortic pressure level. Second, physiological pressures were applied to the aortic root substructures. For further details, we refer the reader to (Conti et al. 2010). This allowed to obtain two reference open leaflets configurations, one for BAV and one for TAV.

In this work, we were interested in computing fluid-dynamic quantities at the systole, since they characterize the abnormal flow in presence of BAV. For this reason, we considered the open configurations obtained by the BAV and TAV structural simulations in the reference geometry and we mapped them into the volumes of the two patients, using Gambit, an Ansys preprocessor for engineering analysis. This mapping has been realized for both patients imposing that the resulting dimension of the BAV orifices and the orien-tation of the valves were the same as those measured from the TrueFisp sequences. This allowed to obtain, for both Patients 1 and 2, a BAV and a TAV open leaflets configuration in the same volume, and then to appreciate the differences induced by the different valves, see Fig. 2.

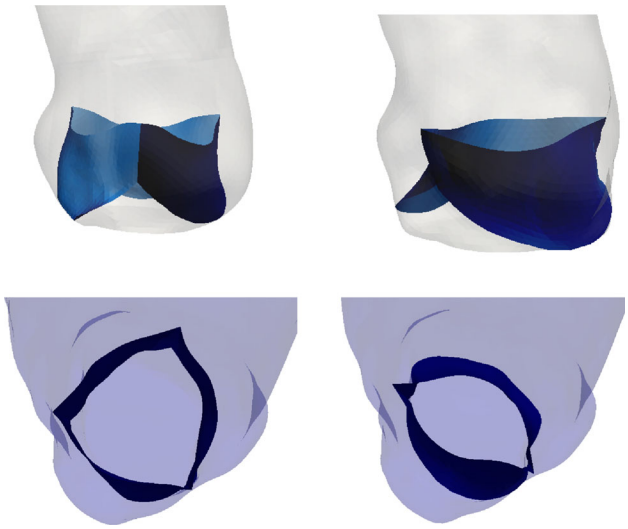

Fig. 2 Valve leaflets for the tricuspid (*left*) and the bicuspid (*right*) configurations. Patient 1

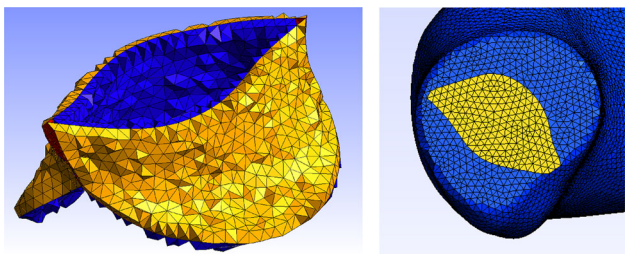

Fig. 3 Mesh of the internal leaflets in the BAV configuration (*left*) and of the projected valve orifice (*right*) Patient 1

2.3 Generation of the meshes

Once we have obtained the four geometries with the open leaflets, we generated with *vmtk* a volume mesh of linear tetrahedra and a conforming superficial mesh for the leaflets, achieving for each of the two patients the computational domains with leaflets for the TAV and BAV cases. In what follows, we refer to such meshes as BAV-leaflets and TAV-leaflets (see Fig. 3, left, for the leaflets mesh).

All leaflets triangles were duplicated, thus obtaining two coinciding surfaces and a discontinuity of the solution through the leaflets.

In order to assess the accuracy of the simulations in presence of the leaflets, we generated for the two BAV cases also the corresponding two meshes without leaflets. To this aim, we identified for each scenario the valve plane. Then, for both patients, we projected onto the valve plane the orifice delimited by the endpoints of the leaflets in the systolic configuration. At the end, two regions were identified on this plane: the bicuspid valve orifice (yellow in Fig. 3, right), which is the inlet for the fluid-dynamic simulations, and an impermeable region (blue in Fig. 3, right). Then, a mesh of

Table 1 Values of the valve orifice areas expressed in cm^2

	Patient 1	Patient 2
TAV-leaflets	3.1	4.2
BAV-leaflets	2.0	2.5
BAV-no-leaflets	1.8	2.3

linear tetrahedra was generated with *vmtk* for each of the two patients, obtaining the computational domains without leaflets. In what follows, we refer to such meshes as BAV-no-leaflets.

In Table 1, we report the values of the orifice area for all the meshes considered.

Concerning the number of elements of each mesh, we obtained about 10^6 tetrahedra and 1.7×10^5 corresponding vertices for all the meshes related to the Patient 1, and about 1.2×10^6 tetrahedra and 2.3×10^5 corresponding vertices for the meshes related to the Patient 2.

These numbers of tetrahedra were chosen after a grid convergence analysis performed according to Celik et al. (2008). In particular, we selected three mesh sizes for Patient 2 corresponding to 0.75×10^6, 1.2×10^6 and 1.6×10^6 tetra-hedra, and we computed the fluid-dynamic indices for these scenarios. The relative errors between the finest and the inter-mediate meshes for all the indices described in Sect. 2.5 were below 3 %. Thus, a number of tetrahedra equal to 1.2×10^6, corresponding to the intermediate mesh, were suitable to have grid independence. This number of tetrahedra corresponds to a space discretization parameter approximatively equal to 0.08 cm, which have been then used also for Patient 1.

2.4 Description of the numerical simulations

Unsteady numerical simulations were performed by using the finite element library LifeV (see www.lifev.org). Blood was considered as Newtonian, homogeneous, and incompress-ible, modeled by the Navier–Stokes equations for incom-pressible fluids (Formaggia et al. 2009). The blood viscosity was 0.035 P, the density was 1.0 g/cm^3, and the time step was 0.01 s. For time independence, we tested that halving the time step the results remained the same up to a suitable tolerance. We used P1-P1 finite elements stabilized with the interior penalty technique, see Burman et al. (2006). The ves-sel wall was considered rigid since we do not expect that the dynamics of the wall substantially affects the abnormal sys-tolic flows, especially the comparisons among the different cases. Being interested in the hemodynamics at systolic ejec-tion, the opening and closure mechanism of the valve leaflets was not modeled in the case with leaflets, since we assumed that this would not influence the direction of the jet at systole and the other fluid-dynamic quantities. Valve opening and closure were therefore modeled in an on/off modality without considering the intermediate steps. For our tests, we prescribed the same standard representative healthy flow rate to both patients (Avolio 1980) (see Fig. 4). To prescribe this flow rate, a Dirichlet boundary condition at the inflow under the assumption of flat velocity profile was imposed (Moireau et al. 2012). At the outlets, a zero-stress condition was prescribed, since the region of interest is in the proximal ascending aorta. It must be highlighted that no turbulence models were assumed.

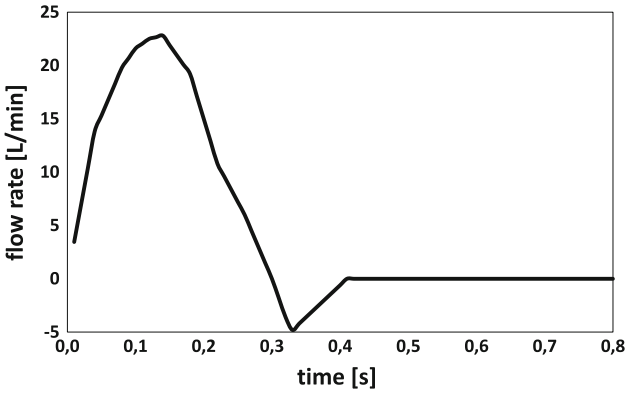

Fig. 4 Representative flow rate curve imposed at the inlet in all the scenarios

2.5 Indices for hemodynamic quantifications

In order to perform a quantitative comparison among the vari-ous configurations, we introduced suitable easily computable indices providing useful information about the abnormal flow in the ascending aorta.

Flow asymmetry BAV configurations lead to an asymmetric systolic flow in the ascending aorta. To quantify this eccentricity, we used the normalized flow asymmetry index NFA proposed in (Sigovan et al. 2011), defined as follows:

$$\mathrm{NFA} = \frac{||\mathbf{c}_S - \mathbf{c}_{\mathrm{vel}}||}{L}, \tag{2}$$

where $\mathbf{c}_{\mathrm{vel}}$ is the center of velocity on S defined as $(\mathbf{c}_{\mathrm{vel}})_j = \frac{\int_S j\mathbf{u}^+ \cdot \mathbf{n} d\sigma}{\int_S \mathbf{u}^+ \cdot \mathbf{n} d\sigma}$, $j = x, y, z$, where $\mathbf{u}^+$ is the part of the velocity $\mathbf{u}$ such that $\mathbf{u}^+ \cdot \mathbf{n} > 0$ on S ($\mathbf{n}$ being the normal direction to the section S), $\mathbf{c}_S$ is the barycenter of the section S and L is a characteristic length of S.

We have NFA = 0 when the center of velocity lies in the center of the vessel (no asymmetric flow) and NFA=1 when it is on the vessel wall (totally asymmetric flow). *Retrograde flow analysis* One of the features of the systolic abnormal flow induced by a BAV configuration is the forma-tion of retrograde flows in the ascending aorta. To quantify them, we introduce the index FRR on a section, defined as follows: (Barker and Markl 2011; Faggiano et al. 2013)

$$\mathrm{FRR} = \frac{|Q_{\mathrm{neg}}(t_{\mathrm{sys}})|}{|Q_{\mathrm{pos}}(t_{\mathrm{sys}})|}\%, \tag{3}$$

where Q_{neg} and Q_{pos} represent the backward and forward flow rates on the section at hand, respectively, and t_{sys} is the systolic instant. Observe that FRR $= 0$ means that no retrograde flow occurred.

Systolic helical flow pattern analysis As observed in the intro-duction, one of the peculiarity of the fluid-dynamics in BAV configurations, strictly related to the formation of retrograde flows and to the jet asymmetry, is the possible formation of helical systolic structures in the ascending aorta at systole, which are completely absent in normal TAV configurations. To quantify such a phenomenon on a section S, in Faggiano et al. (2013), we introduced the positive helix fraction index PHF defined as

$$\mathrm{PHF} = \frac{H_{\mathrm{pos}}}{H_{\mathrm{pos}} + H_{\mathrm{neg}}} \tag{4}$$

where $H_{\mathrm{pos}} = \int_S h^+$, $H_{\mathrm{neg}} = \int_S h^-$, h^+ and h^- are the positive and negative parts, respectively, of the quantity h, defined as

$$h = (\nabla \times ((\mathbf{u}(t_{\mathrm{sys}}) \cdot \boldsymbol{\tau})\boldsymbol{\tau}) \cdot \mathbf{n}, \tag{5}$$

where $\boldsymbol{\tau}$ is the tangent direction to the surface S. h is nothing but the normal component of the systolic vorticity of the velocity parallel to the section S. PHF indicates the ratio between right-handed helices and the totality of the rotating flux (PHF $= 1$ means complete right-handed helical flow, PHF $= 0$ means complete left-handed helical flow, PHF $= 0.5$ means no prevalence of any direction).

Wall shear stresses Strictly related to the formation of asymmetric flows is the production of elevated wall shear stresses in the ascending aorta.

To quantify them, we consider the time-averaged wall shear stress (TAWSS($\boldsymbol{x}$)), which represents the magnitude of the wall shear stress averaged over a complete cardiac cycle (Caruso et al. 2008). In particular, we introduce the index $\mathrm{TAWSS}_{\mathrm{max}}$, representing the maximum in space over the ascending aorta of function TAWSS. We also introduce the $\mathrm{WSS}_{\mathrm{max}}$ index, which is the maximum in space of WSS at the systolic peak (Faggiano et al. 2013).

3 Results

In this section, we report the numerical results obtained for the different configurations we have presented. In the first part, we analyze the velocity field and the values obtained for the indices proposed in Sect. 2.5. In the second part of the section, we present the results of a parametric study obtained by varying the flow rate imposed at the inlet, in order to account for low flow rates often measured in BAV patients (Barker et al. 2012).

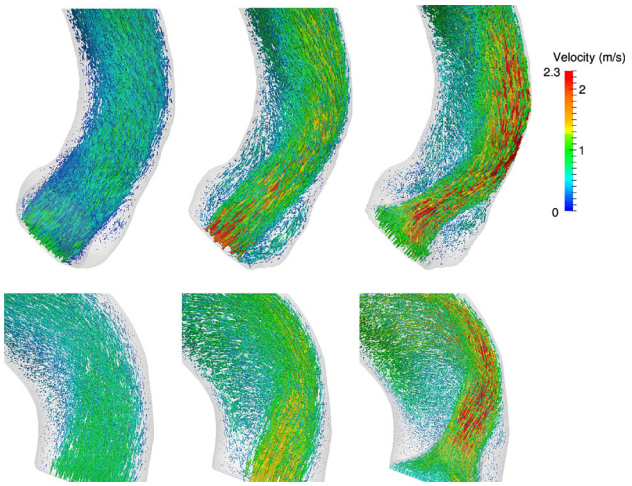

Fig. 5 Velocity field at the systole for Patient 1 (*top*) and Patient 2 (*bottom*). From the *left* to the *right*: TAV-leaflets, BAV-no-leaflets, BAV-leaflets

3.1 Quantification of the indices

3.1.1 Flow asymmetry

In Fig. 5, we show the flow pattern in the ascending aorta at the systole for the three different configurations BAV-leaflets, BAV-no-leaflets, and TAV-leaflets for each patient.

From this figure, we can see a remarkable difference in the fluid-dynamics between the TAV and the BAV cases, for both patients. We notice an asymmetric distribution of the velocity field in the BAV models, in particular, between the valsalva sinus and the mid-ascending aorta, against a symmetric flow for the TAV configurations. In addition, BAV configurations feature higher values of the systolic velocity with respect to TAV. As for the comparison between the two BAV cases, with and without leaflets, we observe that the presence of the leaflets emphasizes the abnormal characteristic of the flow pattern leading to higher values of the velocity and to a more pronounced asymmetry in the ascending aorta for both patients.

In Table 2, the values of the NFA index for all the simulations are reported. We observe that the values obtained for TAV cases are very small, confirming the symmetry of the flow for patients with tricuspid aortic valve. On the contrary, in the BAV cases, the increased value of NFA highlights the deflection of the flow toward the wall, a phenomenon that increases approaching the mid-ascending aorta. In particular, we notice that at the STJ (section A1), there are differences between the cases with and without leaflets of 16 % for Patient 1 and 4 % for Patient 2, whereas at the mid-ascending aorta

Table 2 Values of the index NFA at the sinotubular junction (A1) and at the mid-ascending aorta (A2)

	Patient 1		Patient 2	
	A1	A2	A1	A2
TAV-leaflets	0.054	0.053	0.172	0.084
BAV-no-leaflets	0.196	0.285	0.305	0.336
BAV-leaflets	0.228	0.390	0.317	0.462

Table 3 Values of the index FRR (in %) at the sinotubular junction (A1) and at the mid-ascending aorta (A2)

	Patient 1		Patient 2	
	A1	A2	A1	A2
TAV-leaflets	1.8	0.0	5.02	0.0
BAV-no-leaflets	9.39	0.55	16.45	0.99
BAV-leaflets	11.18	11.56	14.23	10.77

(section A2) NFA values increase by 37 % and 38 % in the model with the leaflets. Finally, we observe that, in all configurations, the asymmetry is more pronounced for Patient 2, which is characterized by a dilated configuration of the ascending aorta.

3.1.2 Retrograde flow

We report in Table 3 the values of the flow reversal ratio FRR for all the simulations. From these results, we notice that in the TAV configurations, there is no retrograde flow at the peak systole, FRR being very small at the STJ and exactly zero at the mid-ascending aorta. A clear increase in FRR in the bicuspid cases is observed. In particular, elevated values of the index occur in all BAV models at both levels A1 and A2, indicating the presence of a recirculation zone. This index features a behavior similar to that of NFA, in the sense that the differences between BAV models with and without leaflets are less pronounced at the STJ (A1) (an increment by 19 % is observed in the case with leaflets for Patient 1 and by 16% in the case without leaflets for Patient 2). On the contrary, at the mid-ascending aorta (A2), the model without leaflets featured very small values of FRR (very close to zero, thus without any substantial retrograde flow), whereas the one with the leaflets experienced high values of FRR and thus a high retrograde flow.

3.1.3 Helical flow analysis

Figure 6 shows the streamlines of the velocity field at the systole for Patient 2.

We note a considerable difference between the TAV and the BAV cases. Indeed, in the TAV configuration, the flux goes straight into the ascending aorta, without creating any secondary flow. On the contrary in the BAV models, the streamlines are not parallel to the wall and we can observe the formation of a vortex with an evident helical pattern (for the BAV-no-leaflets case see also Faggiano et al. (2013)).

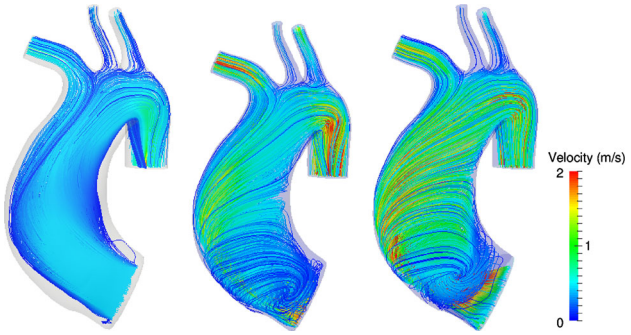

Fig. 6 Streamlines of the velocity field at the systole for Patient 2. From the *left* to the *right*: TAV-leaflets, BAV-no-leaflets, BAV-leaflets

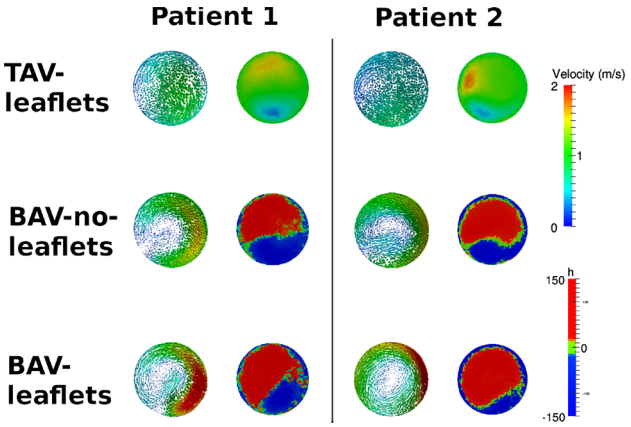

Fig. 7 Top view of the mid-ascending aorta section (A2) with the computed three-dimensional velocity field and the corresponding h values for Patient 1 (*left*) and Patient 2 (*right*). From the *top* to the *bottom*: TAV-leaflets, BAV-no-leaflets, BAV-leaflets. h red colors stand for $h > 0$ (local right-handed helical structure), *blue* colors stand for $h < 0$ (local left-handed helical structure), and *green* colors stand for h = 0 (no local helical structure)

Figure 7 shows the velocity field and the quantity h at the level A2, highlighting the formation of a right-handed vortex for all BAV configurations (absent in the TAV-leaflets case), related to the lateral displacement of the flow and to its asymmetry. For each patient, the two BAV models, with and without leaflets, present comparable results and show the formation of very similar vortices, which, however, are slightly more pronounced in the BAV-leaflet configuration.

In Table 4, we report the values of the PHF index at the mid-ascending aorta. These results confirm that the helical flow is absent for the TAV-leaflets cases (PHF very close to 0.5) and that it is more pronounced in the BAV case with leaflets. In particular, for the BAV cases, PHF increased in the case with leaflets by 22 % for Patient 1 and 14 % for Patient 2. Moreover, they highlight the increased vorticity for

Table 4 Values of index PHF at the mid-ascending aorta (A2)

	Patient 1	Patient 2
TAV-leaflets	0.57	0.60
BAV-no-leaflets	0.59	0.76
BAV-leaflets	0.72	0.87

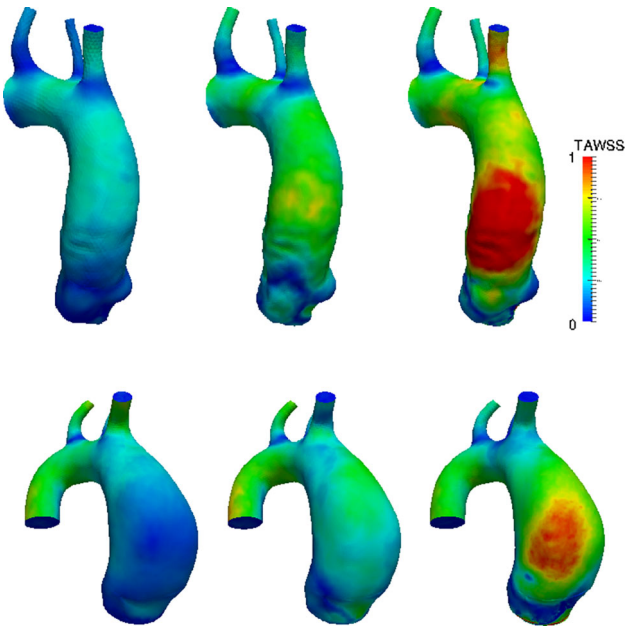

Fig. 8 Time-averaged wall shear stress for Patient 1 (*top*) and Patient 2 (*bottom*) measured in Pascal. From the *left* to the *right*: TAV, BAV without leaflets, BAV with leaflets

Patient 2 with respect to Patient 1 for all the BAV cases. This suggests that the helical pattern is more relevant in case of aortic dilatation, thus confirming for the models with leaflets, what found for the case without leaflets in Faggiano et al. (2013).

3.1.4 Wall shear stress

In Fig. 8, we show the TAWSS for all the simulations performed. We observe a clear increase in the TAWSS values for all BAV configurations with respect to TAV-leaflets cases in the ascending aorta, where most of aortic aneurysms are located. From a comparison between the two different BAV models we see that the leaflets lead to a considerable increase in TAWSS for both patients. In addition, we observe that, in presence of the leaflets, the area with higher values of TAWSS is located at a lower level with respect to the one obtained without leaflets.

Moreover, we report in Table 5 the values of the index $\mathrm{WSS}_{\max}$ and in Table 6 the values of the index $\mathrm{TAWSS}_{\max}$. These results confirm the qualitative observations made above. In particular, $\mathrm{WSS}_{\max}$ ($\mathrm{TAWSS}_{\max}$) in the BAV-leaflets configurations is almost four times bigger than in the TAV-leaflets case and almost twice than in the BAV-no-leaflets configuration.

Table 5 Values of the index $\mathrm{WSS}_{\max}$

	Patient 1	Patient 2
TAV-leaflets	1.21	1.03
BAV-no-leaflets	2.86	2.06
BAV-leaflets	4.71	3.71

Table 6 Values of the index $\mathrm{TAWSS}_{\max}$

	Patient 1	Patient 2
TAV-leaflets	0.32	0.26
BAV-no-leaflets	0.75	0.57
BAV-leaflets	1.57	1.09

3.2 Parametric flow rate analysis

Often, in BAV configurations, the flow rate entering the aorta through the aortic valve is lower than the one occurring in a normal tricuspid case, because of recurring stenosis (Barker and Markl 2011). In our cases, Patient 1 featured a mild stenotic valve. This justified a sensitivity analysis to inves-tigate the dependence of the proposed indices on maximum value of the flow rate. In particular, we performed the numer-ical simulations for all the BAV cases, by prescribing a flow rate at the inlet which is equivalent to $\frac{2}{3}$ of the previous one, with a mean flow rate decreasing from 4,85 to 3,23 l/min. We refer to the standard and lower flow rates as $F1$ and $F2$, respectively.

In Tables 7, 8, 9, and 10, we compare the values of the indices obtained with the original flow rates and with the reduced one, for both patients. We notice that the values of indices NFA and PHF related to the BAV model with the leaflets obtained with the lower flow rate $F2$ are in general

Table 7 Values of index NFA at the STJ (A1) and at the mid-ascending aorta (A2)

	Patient 1		Patient 2	
	A1	A2	A1	A2
$F1$				
BAV-no-leaflets	0.196	0.285	0.305	0.336
BAV-leaflets	0.228	0.390	0.317	0.462
$F2$				
BAV-no-leaflets	0.090	0.179	0.291	0.239
BAV-leaflets	0.217	0.364	0.336	0.498

Flow rate parametric study

Table 8 Values of the index FRR at the STJ (A1) and at the mid-ascending aorta (A2)

	Patient 1		Patient 2	
	A1	A2	A1	A2
$F1$				
BAV-no-leaflets	9.39	0.55	16.45	0.99
BAV-leaflets	11.18	11.56	14.23	10.77
$F2$				
BAV-no-leaflets	9.44	0.18	17.71	0.04
BAV-leaflets	12.77	11.03	12.18	20.22

Flow rate parametric study

Table 9 Values of the index PHF at the mid-ascending aorta (A2)

	Patient 1	Patient 2
$F1$		
BAV-no-leaflets	0.59	0.76
BAV-leaflets	0.72	0.87
$F2$		
BAV-no-leaflets	0.55	0.56
BAV-leaflets	0.71	0.84

Flow rate parametric study

Table 10 Values of the WSSmax index

	Patient 1	Patient 2
$F1$		
BAV-no-leaflets	2.86	2.06
BAV-leaflets	4.71	3.71
$F2$		
BAV-no-leaflets	1.27	1.17
BAV-leaflets	3.18	2.49

Flow rate parametric study

very similar to those obtained with $F1$. On the contrary, we observe a marked difference among the results obtained with the two flow rates for the BAV-no-leaflets models, especially for NFA and PHF. In particular, in this case, the abnormalities of the fluid-dynamics are strongly reduced with the lower flow rate, leading to a jet which is more symmetric and characterized by a small right-handed helical structure.

4 Discussion

4.1 State of the art and choice of the computational model

The study of the fluid-dynamics in the ascending aorta in presence of a bicuspid aortic valve by means of computational tools is a quite recent topic. To our knowledge, the first work in this direction has been provided by Richards et al (2004), where the authors considered 3D simulations in idealized rigid geometries, without any modelization of the leaflets. A similar investigation has been then provided in Donal et al. (2005a). The first studies with patient-specific geometries have been reported in Viscardi et al.(2010) and LaDisa et al. (2010), where, however, the leaflets are not modeled and the valve orifice has been projected on the valve plane. Similar investigations have been then provided in Tse et al. (2011), Vergara et al. (2012), Fag-giano et al. (2013), Wendell et al. (2013). Other works considered the fluid–structure interaction arising between the blood and the aorta wall, we mention Weinberg and Kaazempur Mofrad (2008), Chandra et al. (2012), and Marom et al. (2013a) for the case of idealized geome-tries, and Pasta et al. (2013) for patient-specific geome-tries.
As for the modelization of the leaflets in the BAV con-text, their inclusion without modeling their movement has been considered in Della Corte et al. (2012) and Pasta et al.(2013), whereas two-dimensional (Chandra et al. 2012) or simplified (Weinberg and Kaazempur Mofrad 2008; Marom et al. 2013a) modeling of the interaction between blood and leaflets have been also considered. Although in the recent years, an increasing number of works has been studying the modeling of the interaction between blood and leaflets for the tricuspid and mechanical bileaflets cases (see, e.g., Borazjani et al. (2010), Borazjani and Sotiropoulos (2010), Borazjani (2013), Le and Sotiropoulos (2013)), in the BAV case, a complete three-dimensional model is still miss-ing.

In this work, we considered numerical simulations in patient-specific geometries with the presence of the leaflets, to assess the influence of the latter in the fluid-dynamics. In particular, we did not model the interaction between the blood and the leaflets; instead, we built two reference open configurations of the leaflets (one for TAV and one for BAV) by solving structural simulations based on the average of some patient-specific data, and then we mapped them into the patient-specific geometries. This choice has been done, as a first approximation, since here we were interested in simulating the fluid-dynamics at the systole, when the leaflets are completely open. Our aim was to perform a compari-son with other configurations (BAV without leaflets, TAV with leaflets). In this respect, we believe that the complete opening/closure mechanism of the valve should not have a significant influence on the comparison of the systolic fluid-dynamic quantities. Moreover, we assumed a rigid aortic wall. Again, this simplifying hypothesis has been justified by observing that the description of the interaction between blood and vessel should not influence the comparison performed in this work.

4.2 Abnormal fluid-dynamics induced by a bicuspid configuration

As highlighted in the Introduction, the fluid-dynamics in the ascending aorta in presence of a non-stenotic bicuspid aortic valve is very different from the one developing in a TAV configuration. In particular, BAV configurations are characterized by a pronounced asymmetry of the systolic jet entering the aorta, which generates large zones of flow rever-sal, high WSS at the sinotubular junction and mid-ascending aorta, and, often, systolic helicoidal patterns. The computa-tional studies mentioned above described such abnormalities. In particular, the asymmetry of the jet has been firstly reported by the results in Donal et al. (2005b), where, however, the authors prescribed a priori the angle between the jet direction and the longitudinal axis. Then, this phenomenon has been recovered without any a priori imposition on the jet angle by the results in Viscardi et al. (2010), Tse et al. (2011), Vergara et al. (2012), Faggiano et al. (2013), and Pasta et al. (2013), for the case without leaflets, and in Della Corte et al. (2012), Marom et al. (2013a) and Chandra et al. (2012) in presence of the leaflets. Moreover, in vivo evidences of flow asymmetry and sistolic helical flows have been reported in Barker et al.(2012), Hope et al. (2011). The abnormal maximum WSS in the ascending aorta has been reported by the results in Vis-cardi et al. (2010) , LaDisa et al. (2010), Tse et al. (2011), and Pasta et al. (2013), whereas the formation of flow rever-sals and systolic vortices in Tse et al. (2011), Chandra et al. (2012), Faggiano et al. (2013), and Marom et al. (2013a).

4.3 Comparison among different configurations

BAV-leaflets versus BAV-no-leaflets The numerical studies mentioned above suggested that the asymmetry of the systolic jet and the fluid-dynamic abnormalities observed in BAV configurations are provoked by two independent factors: (1) The shape of the open BAV orifice in combination with the typical curvature and torsion of the ascending aorta; (2) The presence of the BAV-leaflets in the open configuration, which forces the jet direction.

In this work, we tried to quantify these two separate contributions. To do this, we compared the numerical results obtained with and without the inclusion of the leaflets in BAV computational models. In particular, the comparison has been performed in two real geometries of the ascending aorta, a non-dilated one, and a dilated one.

The results reported in Tables 2, 3, 4, 5, and 6 showed that, for both patients, jet asymmetry, flow reversal, formation of helicoidal patterns and WSS increase at the systole when the leaflets are modeled. We also notice that the values of the time-averaged WSS notably increase. This is of particular interest, since it is known that regions of high TAWSS may cause degenerative lesions of the aortic wall, thus predisposing the dilatation process (Tan et al. 2009). Physiological values of TAWSS in the ascending aorta are commonly less than 1 Pa (Tan et al. 2009; Lantz et al. 2011). In our case, we obtained maximum values of 1.57 and 0.75 Pa for the case with and without leaflets, respectively. This implies that without modeling the leaflets, we could not be able to detect the risk of degenerative lesions.

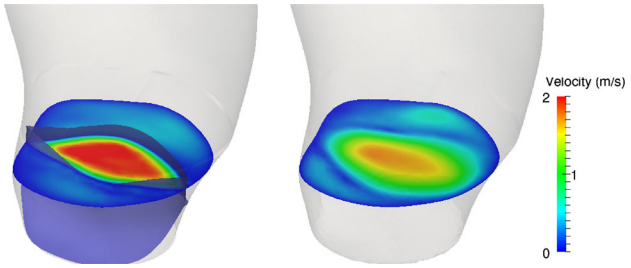

Fig. 9 Velocity field on a selected section just below the endpoints of the leaflets in the BAV-leaflets configuration (*left*) and on the same section in the BAV-no-leaflets configuration (*right*)

The increment of the indices quantifying the abnormal flow observed when the leaflets are included in the computational models could be explained by observing Fig. 9. In particular, in this figure, the systolic velocity field on a representative section located just below the plane given by the endpoints of the leaflets is reported for the BAV-leaflets configuration, together with the systolic velocity field on the same section obtained with the BAV-no-leaflets configuration. These plots highlight that the systolic jet is confined in a small region in the BAV-leaflets case due to the presence of the leaflets, whereas it is more spread out in the configuration without leaflets, since in this case, the blood flowing between the valve orifice and the section at hand could diffuse in a wider region. This emphasizes the jet asymmetry (and thus the other abnormalities) in the case with leaflets at the STJ and, in particular, at the mid-ascending aorta level. This is in agreement with the fact that the inclusion of the leaflets produces a greater increment at the mid-ascending aorta with respect to the STJ for the NFA and FRR indices.

These results also suggest that the inclusion of the leaflets is important to describe the abnormal fluid-dynamics for BAV patients, especially for the non-dilated configuration (Patient 1), which presents a greater increment of the indices, see per-centages reported in Sect. 3.1. Probably, the greater volume of the ascending aorta in the dilated case facilitates the forma-tion of a pronounced jet asymmetry also without modeling the leaflets. This induces the formation of a vortex generated by the pressure difference occurring in the dilated region between the jet and the empty region. In the non-dilated case, this dynamics is less pronounced and the inclusion of the leaflets becomes more influential for the generation of the jet asymmetry and of the other abnormalities.

BAV-leaflets versus TAV-leaflets The comparison between the fluid-dynamics in BAV and TAV cases with leaflets has been reported in several works. We mention Hope et al. (2010, 2011), Barker and Markl (2011) among the radiological studies, Pasta et al. (2013) as computational study in real geometries in presence of the leaflets, and Saikrishnan et al.(2012) among the in-vitro studies.

Our results allowed to compare the fluid-dynamics in the TAV and in the BAV cases in presence of the leaflets, confirm-ing the findings of the above works. In all the cases, the value of the indices increased notably in the BAV case. In particu-lar, the NFA index was below 0.085 in the TAV-leaflets cases (except for a value of 0.172 at the STJ of Patient 2), support-ing the thesis of a centered flow for TAV configurations also in presence of the leaflets. On the contrary, for the BAV-leaflets cases, it was always greater than 0.2 with a maximum of 0.46 at mid-ascending level of Patient 2. The FRR was almost always equal to 0.0 % in TAV-leaflets cases with a peak of 5.02 % at the STJ of Patient 2, whereas it assumed values around 11 % in BAV-leaflets, demonstrating the appearance of retrograde flow only in BAV. The PHF assumed values near 0.5 in TAV-leaflets (absence of any prevalence between right and left handed flows), whereas it increased to 0.72 for Patient 1 and 0.87 for Patient 2 in BAV-leaflets cases, denoting a clear presence of a right-handed flow. Also, WSS values became at least three times greater in BAV-leaflets cases with respect to TAV-leaflets. These results highlighted that, also in presence of the leaflets, the fluid-dynamics in presence of BAV is very different from the one with TAV, which features a symmetric systolic jet, very low flow reversals, and no helicoidal patterns at the systole, thus confirming what found in previous works for the case without leaflets, see, e.g., Vergaraetal.(2012). *Flow rate parametric study* Tables 7, 8, 9, 10 report the results obtained with a smaller flow rate prescribed at the inlet. These simulations have been carried out to define the influence of valve leaflets in presence of a reduced flow rate due for example to a mild aortic valve stenosis (as hap-pens for Patient 1), a common situation for BAV patients. In fact, clinically relevant scenarios include patients with mildly or moderately stenotic BAV, with or without asso-ciated ascending aortic dilatation, either in natural history subject to follow-up imaging investigations or as result of surgical repair of regurgitant BAV (Luciani et al. 2012).

Passing from the original to the lower flow rate, NFA was nearly the same in BAV-leaflets, whereas it decreased substantially in BAV-no-leaflets, assuming values similar to those of TAV-leaflets for the original flow rate; FRR increased in BAV-leaflets cases, whereas it remained nearly constant in BAV-no-leaflets with only one case in which it decreased; PHF, became nearly 0.5 for BAV-no-leaflets cases, indicating the loss of a prevalent helical structure, whereas in BAV-leaflets cases, it decreased, however, demonstrating a clear prevalence of a right-handed helix; WSS_{max} decreased substantially for all the configurations, maintaining higher values (almost two times greater) in BAV-leaflets with respect to BAV-no-leaflets. From these results, we conclude that, in case of mild valve dysfunction, only the shape of the valve orifice in combination with the particular geometry of the ascend-ing aorta is not able to reproduce all the abnormalities of the fluid-dynamics. Thus, we recommend the inclusion of the leaflets in particular in presence of small flow rates.

4.4 Do leaflets provide more reliable results?

The results reported in this work for the BAV configurations highlighted a general tendency to have more pronounced fluid-dynamics abnormalities in the case where the leaflets are modeled with respect to the case where the valve orifice is projected on the valve plane and the leaflets are neglected. The question now is whether leaflets inclusion gives more accurate results. Of course, our expectation is that the model with the leaflets should provide more reliable results, since the physical phenomenon is described in a more accurate way.

To support this observation, we report here very preliminary results about the comparison with measured data. In particular, we considered for Patient 2 a slice (called *PC-slice*) positioned at the mid-ascending aorta approximately at 2 cm from the most distal part of the sinotubular junction, see Fig. 10, left. On this slice, we acquired a 2D CINE PC-MRI acquisition (see Appendix for more details). As inflow condition for the numerical simulations, we imposed the patient-specific flow rate measured by the PC-MRI data (see Fig. 10, right).

In Fig. 11, we show a top view of the PC-slice where the velocity field and the h distribution are reported. We can see that both BAV models recognize the presence of a right-handed vortex, showing a pattern that is, on a qualitative level, very similar to the measures, especially for the model with the leaflets.

In Table 11, we reported the values of NFA, FRR, and PHF obtained at the PC-slice with our BAV simulations and with the 2D CINE PC-MRI acquisition.

These results showed that for all the indices, there is a better agreement with the measures when the leaflets are

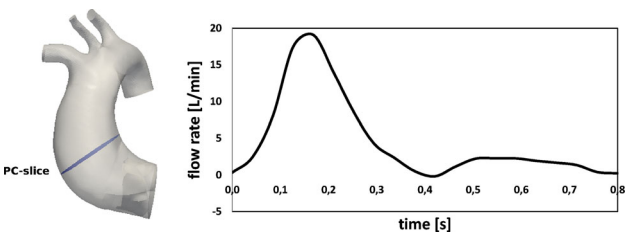

Fig. 10 Location of the PC-slice for Patient 2 (*left*) and patient-specific inlet flow rate obtained by PC-MRI acquisitions (*right*)

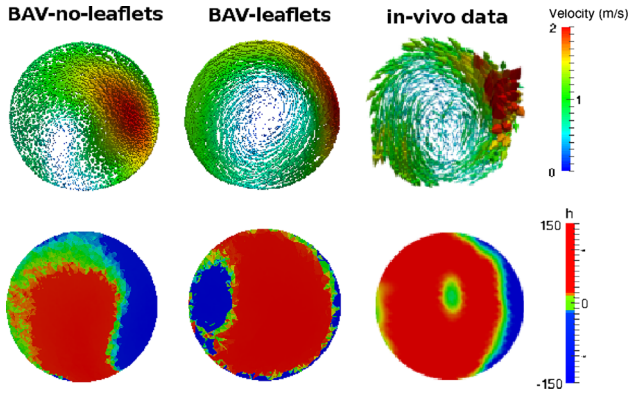

Fig. 11 Velocity field (*top row*) and h distribution (*bottom row*) on the PC-slice. From left to right: BAV-no-leaflets, BAV-leaflets, in-vivo data

Table 11 Indices NFA, FRR, and PHF computed on the PC-slice

	NFA	FRR	PHF
BAV-no-leaflets	0.37	9.1	0.69
BAV-leaflets	0.52	27.2	0.83
In vivo	0.59	46.7	0.82

modeled. In particular, NFA and PHF indices are almost identical, whereas FRR index is still far from the real value. This could be ascribed to two reasons: (1) the absence in our models of the interaction with the aortic wall, producing a possible underestimation of the flow reversal due to the aortic dilatation and (2) the numerical dissipation which tends to soften the secondary flows. Since PHF index is in good agreement with the measures, we have a propensity to think that the main reason of the discrepancy observed for FRR index is due to the absence of a fluid-structure interaction model.

This comparison, although far to be a definitive validation, showed that the increment observed for all the indices quantifying the fluid-dynamic abnormalities seems to be in the direction of a better description of the physical phenomena, thus providing a preliminary step toward a validation of our results.

5 Conclusions and limitations

In previous works, it had been shown that the particular valve orifice shape in BAV configurations, in combination with the typical curvature and torsion of the aorta, was enough to reproduce the fluid-dynamic abnormalities absent in the TAV cases. In this paper, we showed that the inclusion of the leaflets in computational models canalizes the systolic jet, emphasizing the abnormalities of BAV flow, also in presence of failure. This has been proved by a preliminary validation with in vivo data. In particular, we found that the inclusion of the leaflets is recommended to describe:

- Non-dilated ascending aortas;
- Cases with a reduced flow rate (as happens for stenotic BAV);
- Fluid-dynamic abnormalities at the mid-ascending aorta level.

The first limitation of this study concerns the clinical data acquired. Indeed, we did not have available the patient-specific configurations of the leaflets. Nowadays, with the modern image acquisition techniques, it is possible to acquire this information, in particular, for ad hoc studies. However, common clinical procedures often do not allow to have the adequate spatial and temporal resolution to detect the leaflets. Then, our work could provide concrete indications for those studies where no patient-specific leaflets are available.

Other limitations are related to the physical and computational models chosen for this study. First of all, we made a rigid wall assumption, thus neglecting the interaction between fluid and aortic wall structure, and we did not consider an open/closure mechanism of the valve. As observed, this could be the cause of the significant underestimation of FRR index also in presence of the leaflets. We also neglected the presence of the ventricle which can influence the direction of the flow through the valves, in particular by inducing rotational patterns due to the heart torsion. This was due to the lack of data on the ventricle geometry and of a suitable fluid-structure interaction model in the ventricle, which needs ad hoc strategies to be accurately simulated. In any case, we observe that the PC-MRI data showed a velocity pattern which seems to be orthogonal to the valve plane.

Furthermore, we did not consider any turbulence or transition model, which is probably necessary in the ascending aorta (see Saikrishnan et al. (2014) for an experimental study). In particular, the maximum Reynolds number characterizing our simulations was 4000 for Patient 1 and 5000 for Patient 2. As discussed, we do not believe that the inclusion of these features in our computations affects the final conclusions of the work, since this is a comparative study. However, the improvement of the physical and computational models will allow to obtain even more accurate indications about the fluid-dynamics in presence of BAV, so that we are working for future studies on these topics.

Acknowledgments This work has been partially supported the Italian MIUR PRIN12 project n. 201289A4LX. The numerical simulations have been performed at CINECA Consortium through the LISA Projects LI02p-FSIA2 and Lisa Project LI02p- LEScarot.

6 Appendix

We provide here some technical details on the 2D CINE PC-MRI acquisition made for Patient 2 at the PC-slice. A

1.5 Tesla system (Magnetom Symphony, Siemens Medical Systems, Erlangen, Germany) has been used. The temporal resolution was characterized by 20 phases in one cardiac cycle with a pixel resolution of 1.17×1.17 mm. Velocity encoding values were chosen to optimize the velocity map resolution with a value equal to 150 cm/s. The following parameters were also used: TE (echo time) = 6.4 ms; flip angle = 15°; slice thickness = 5 mm; acquisition matrix = 256×256.

References

Atkins S, Cao K, Rajamannan N, Sucosky P (2014) Bicuspid aortic valve hemodynamics induces abnormal medial remodeling in the convexity of porcine ascending aortas. Biomech Model Mechanobiol 13(6):1209–1225

Avolio P (1980) Multi-branched model of the human arterial system. Med Biol Eng Comput 18(6):709–718

Barker A, Markl M (2011) The role of hemodynamics in bicuspid aortic valve disease. Eur J Cardiothorac Surg 39(6):805–806

Barker A, Lanning C, Shandas R (2010) Quantification of hemodynamic wall shear stress in patients with bicuspid aortic valve using phase-contrast mri. Ann Biomed Eng 38(3):788–800

Barker A, Markl M, Burk J, Lorenz R, Bock J, Bauer S, Schulz-Menger J, Von Knobelsdorff-Brenkenhoff F (2012) Bicuspid aortic valve is associated with altered wall shear stress in the ascending aorta. Circ Cardiovasc Imag 5(4):457–466

Bauer M, Siniawski H, Pasic M, Schaumann B, Hetzer R (2006) Different hemodynamic stress of the ascending aorta wall in patients with bicuspid and tricuspid aortic valve. J Card Surg 21(3):218–220

Billiar K, Sacks M (2000) Biaxial mechanical properties of the natural and glutaraldehyde treated aortic valve cusp—part I: Experimental results. J Biomech Eng 122(1):23–30

Borazjani I, Ge L, Sotiropoulos F (2010) High-resolution fluid-structure interaction simulations of flow through a bi-leaflet mechanical heart valve in an anatomic aorta. Ann Biomed Eng 38(2):326–344

Borazjani I, Sotiropoulos F (2010) The effect of implantation orientation of a bileaflet mechanical heart valve on kinematics and hemodynamics in an anatomic aorta. J Biomech Eng 132(11):111005

Borazjani I (2013) Fluid-structure interaction, immersed boundary-finite element method simulations of bio-prosthetic heart valves. Comput Methods Appl Mech Eng 253:103–116

Burman E, Fernandez M, Hansbo P (2006) Continuous interior penalty finite element method for Oseen's equations. SIAM J Numer Anal 44(3):1248–1274

Caruso MV, Gramigna V, Rossi M, Serraino GF, Renzulli A, Fragomeni G (2015) A computational fluid dynamics comparison between different outflow graft anastomosis locations of Left Ventricular Assist Device (LVAD) in a patient-specific aortic model. Int J Numer Methods Biomed Eng 31(2)

Celik IB, Ghia U, Roache PJ, Freitas CJ, Coleman H, Raad PE (2008) Procedure for estimation and reporting of uncertainty due to discretization in CFD applications. J Fluids Eng Trans ASME 130:1–4

Chandra S, Rajamannan N, Sucosky P (2012) Computational assessment of bicuspid aortic valve wall-shear stress: Implications for calcific aortic valve disease. Biomech Model Mechanobiol 11(7):1085–1096

Conti C, Della Corte A, Votta E, Del Viscovo L, Bancone C, De Santo L, Redaelli A (2010) Biomechanical implications of the congenital bicuspid aortic valve: a finite element study of aortic root function from in vivo data. J Thor Cardiovasc Surg 140(4):890–896

Della Corte A, Bancone C, Conti C, Votta E, Redaelli A, Del Viscovo L, Cotrufo M (2012) Restricted cusp motion in right-left type of bicuspid aortic valves: a new risk marker for aortopathy. J Thorac Cardiovasc Surg 144(2):360–369

Den Reijer P, Sallee D, Van Der Velden P, Zaaijer E, Parks W, Ramamurthy S, Robbie T, Donati G, Lamphier C, Beekman R, Brummer M (2010) Hemodynamic predictors of aortic dilatation in bicuspid aortic valve by velocity-encoded cardiovascular magnetic resonance. J Cardiovasc Magn Reson 12(1)

Donal E, Novaro G, Deserrano D, Popovic Z, Greenberg N, Richards K, Thomas J, Garcia M (2005a) Planimetric assessment of anatomic valve area overestimates effective orifice area in bicuspid aortic stenosis. J Am Soc Echocardiogr 18(12):1392–1398

Donal E, Raud-Raynier P, Coisne D, Allal J, Herpin D (2005b) Tissue doppler echocardiographic quantification. Comparison to coronary angiography results in acute coronary syndrome patients. Cardiovasc Ultrasound 3(10)

Faggiano E, Antiga L, Puppini G, Quarteroni A, Luciani G, Vergara C (2013) Helical flows and asymmetry of blood jet in dilated ascending aorta with normally bicuspid valve. Biomech Model Mechanobiol 12(4):801–813

Fedak P, Verma S, David T, Leask R, Weisel R, Butany J (2002) Clinical and pathophysiological implications of a bicuspid aortic valve. Circulation 106(8):900–904

Formaggia L, Quarteroni A, Veneziani A (2009) Cardiovascular mathematics, modeling and simulation of the circulatory system, vol 1. Springer, Berlin

Girdauskas E, Borger M, Secknus M, Girdauskas G, Kuntze T (2011) Is aortopathy in bicuspid aortic valve disease a congenital defect or a result of abnormal hemodynamics? A critical reappraisal of a one-sided argument. Eur J Cardiothorac Surg 39(6):809–815

Girdauskas E, Disha K, Borger MA, Kuntze T (2012) Relation of bicuspid aortic valve morphology to the dilatation pattern of the proximal aorta: focus on the transvalvular flow. Cardiol Res Pract 1(1)

Guntheroth WG (2008) A critical review of the American college of cardiology/American heart association practice guidelines on bicuspid aortic valve with dilated ascending aorta. Am J Cardiol 102:107–110

Hahn R, Roman M, Mograder A, Devereux R (1992) Association of aortic dilation with regurgitant, stenotic and functionally normal bicuspid aortic valves. J Am Coll Cardiol 19(2):283–288

Hope M, Hope T, Meadows A, Ordovas K, Urbania T, Alley M, Higgins C (2010) Bicuspid aortic valve: four-dimensional mr evaluation of ascending aortic systolic flow patterns. Radiology 255(1):53–61

Hope M, Hope T, Crook S, Ordovas K, Urbania T, Alley M, Higgins C (2011) 4D flow CMR in assessment of valve-related ascending aortic disease. JACC Cardiovasc Imaging 4(7):781–787

Hope M, Sigovan M, Wrenn S, Saloner D, Dyverfeldt P (2014) MRI hemodynamic markers of progressive bicuspid aortic valve-related aortic disease. J Magn Reson Imaging 40(1):140–145

Keshavarz-Motamed Z, Garcia J, Gaillard E, Capoulade R, Le Ven F, Cloutier G, Kadem L, Pibarot P (2014) Non-invasive determination of left ventricular workload in patients with aortic stenosis using magnetic resonance imaging and doppler echocardiography. PLoS One 9(1)

LaDisa J, Taylor C, Feinstein J (2010) Aortic coarctation: recent developments in experimental and computational methods to assess treatments for this simple condition. Prog Pediatr Cardiol 30(1–2):45–49

Lantz J, Renner J, Karlsson M (2011) Wall shear stress in a subject specific human aorta—influence of fluid-structure interaction. Int J Appl Mech 759(3)

Le TB, Sotiropoulos F (2013) Fluid-structure interaction of an aortic heart valve prosthesis driven by an animated anatomic left ventricle. J Comput Phys 244(1):44–62

Luciani G, De Rita F, Lucchese G, Hila D, Rungatscher A, Faggian G, Mazzucco A (2012) Repair of congenitally dysplastic aortic valve

by bicuspidization: midterm results. Ann Thorac Surg 94(4):1173–1179

Marom G, Haj-Ali R, Rosenfeld M, SchÃd'fers H, Raanani E (2013a) Aortic root numeric model: annulus diameter prediction of effective height and coaptation in post-aortic valve repair. J Thorac Cardiovasc Surg 145(2):406–411

Marom G, Kim HS, Rosenfeld M, Raanani E, Haj-Ali R (2013b) Fully coupled fluid-structure interaction model of congenital bicuspid aortic valves: effect of asymmetry on hemodynamics. Med Biol Eng Comput 51(8):839–848

May-Newman K, Yin F (1998) A constitutive law for mitral valve tissue. J Biomech Eng 120(1):38–47

Moireau P, Xiao N, Astorino M, Figueroa C, Chapelle D, Taylor C, Gerbeau JF (2012) External tissue support and fluid-structure simulation in blood flows. Biomech Model Mechanobiol 11(1–2):1–18

Nkomo V, Enriquez-Sarano M, Ammash N, Melton L, Bailey K, Desjardins V, Horn R, Tajik A (2003) Bicuspid aortic valve associated with aortic dilatation. Arterioscler Thromb Vasc Biol 23(2):351–356

Pasta S, Phillippi J, Gleason T, Vorp D (2012) Effect of aneurysm on the mechanical dissection properties of the human ascending thoracic aorta. J Thorac Cardiovas Surg 143(2):460–467

Pasta S, Rinaudo A, Luca A, Pilato M, Scardulla C, Gleason T, Vorp D (2013) Difference in hemodynamic and wall stress of ascending thoracic aortic aneurysms with bicuspid and tricuspid aortic valve. J Biomech 46(10):1729–1738

Saikrishnan N, Yap C, Milligan N, Vasilyev N, Yoganathan A (2012) In vitro characterization of bicuspid aortic valve hemodynamics using particle image velocimetry. Ann Biomed Eng 40:1760–1775

Saikrishnan N, Mirabella L, Yoganathan A (2014) Bicuspid aortic valves are associated with increased wall and turbulence shear stress levels compared to trileaflet aortic valves. Biomech Model Mechanobiol. doi:10.1007/s10237-014-0623-3

Schapira J, Martin R, Fowles R (1979) Two dimensional echocardiographic assessment of patients with bioprosthetic valves. Am J Cardiol 43(3):510–519

Sigovan M, Hope M, Dyverfeldt P, Saloner D (2011) Comparison of four-dimensional flow parameters for quantification of flow eccentricity in the ascending aorta. J Magn Reson Imaging 34(5):1226–1230

Tan FPP, Borghi A, Mohiaddin RH, Wood NB, Thom S, Xu XY (2009) Analysis of flow patterns in a patient-specific thoracic aortic aneurysm model. Comput Struct 87(11):680–690

Tse K, Chiu P, Lee H, Ho P (2011) Investigation of hemodynamics in the development of dissecting aneurysm within patient-specific dissecting aneurismal aortas using computational fluid dynamics (CFD) simulations. J Biomech 44(5):827–836

Vergara C, Viscardi F, Antiga L, Luciani G (2012) Influence of bicuspid valve geometry on ascending aortic fluid dynamics: a parametric study. Artif Organs 36(4):368–378

Viscardi F, Vergara C, Antiga L, Merelli S, Veneziani A, Puppini G, Faggian G, Mazzucco A, Luciani G (2010) Comparative finite element model analysis of ascending aortic flow in bicuspid and tricuspid aortic valve. Artif Organs 34(12):1114–1120

Weinberg E, Kaazempur Mofrad M (2008) A multiscale computational comparison of the bicuspid and tricuspid aortic valves in relation to calcific aortic stenosis. J Biomech 41(16):342–348

Wendell DC, Samyn MM, Cava JR, Ellwein LM, Krolikowski MM, Gandy KL, Pelech AN, Shadden SC, LaDisa JF (2013) Including aortic valve morphology in computational fluid dynamics simulations: initial findings and application to aortic coarctation. Med Eng Phys 35(6):723–735